Copper and nickel co-doping effects on the structural, optical and electrical properties of tungsten trioxide nanoparticles prepared by co-precipitation technique

To cite this article: Wegene Lema Lachore *et al* 2022 *Mater. Res. Express* **9** 035008

Materials Research Express

PAPER

Copper and nickel co-doping effects on the structural, optical and electrical properties of tungsten trioxide nanoparticles prepared by co-precipitation technique

Wegene Lema Lachore[1], **Fekadu Gashaw Hone**[2,*], **Dinsefa Mensur Andoshe**[3], **Newayemedhin A Tegegne**[2] **and Mulualem Abebe Mekonnen**[1]

[1] Faculty of Materials Science and Engineering, Jimma Institute of Technology, Jimma University, PO Box: 1041, Jimma, Ethiopia
[2] Department of Physics, Addis Ababa University, PO Box: 1176, Addis Ababa, Ethiopia
[3] Department of Materials Science and Engineering, Adama Science and Technology University, PO Box: 1888, Adama, Ethiopia
[*] Author to whom any correspondence should be addressed.

E-mail: fekeye@gmail.com

Keywords: WO_3, optical properties, electoral properties, codoping, coprecipitation

OPEN ACCESS

RECEIVED
11 February 2022

REVISED
11 March 2022

ACCEPTED FOR PUBLICATION
17 March 2022

PUBLISHED
31 March 2022

Abstract

The pristine WO_3 (tungsten trioxide) and Cu/Ni Co-doped WO_3 nanoparticles were synthesized by the co-precipitation synthesis methods with fixed wt.% of nickel, i.e., 5 wt.%, and different wt.% of copper, i.e., 2, 3, 5 wt.%. The structural, optical and electrical properties, as well as the surface morphology were investigated thoroughly by various characterization techniques. All the doped/co-doped and un-doped samples had an orthorhombic structure, according to the XRD measurements. The XRD results further confirmed that the average crystalline size ranged from 46 to 25 nm after the dopant concentration was introduced. Reflectance spectroscopy was used to investigate the optical properties of the prepared nanomaterials and revealed that the optical band gap varied from 2.80 to 2.63 eV with dopant concentrations. The room temperature photoluminescence study showed that the emission peaks were observed in the visible region with slight peak shift towards short wavelength with dopant concentrations. The FTIR studies described the different mode of band related to a functional groups present in the materials and the stretching mode of O–W–W observed from 550 to 1050 cm^{-1}. The I-V studies confirmed that the prepared samples had a good ohmic contact behavior and the resistivity decreased from $6.3 \times 10^{-3}\Omega$.cm to $0.63 \times 10^{-3}\,\Omega$.cm with doping concentrations.

1. Introduction

Metal oxide semiconductor nanoparticles have recently received a lot of consideration due to their unique potential for different applications. Tungsten trioxide has been highly studied because of its outstanding optical, structural and electrical properties [1]. It has reasonable amount of electrons in the valence band with band gap energy of 2.7 to 3.5 eV [2] and with significant absorption in the far-ultraviolet and visible regions. It has transition metal oxide semiconductor which is an excellent property for various applications, such as photovoltaic [3], electrochromic [4], photocatalyst [5], and photochromic [6], and gas sensor [7]. Various researchers have prepared tungsten trioxide nanostructures such as nanowires, nanotubes, nanoribbons, nanorods, and nanoplates which may influence their physical, optical and electrical properties [8–10]. Controlling the size, surface morphology, and dopant concentration of WO_3 are important to for different applications. Doping is one of the most essential mechanisms to increase material's optical and electrical properties. This means that increasing the materials' conductivity and the optical band gap of the host materials reduces or increases their energy. According to a recent study, substitutional doping of metal ions is a good way to adjust the electronic structure and electrical properties of WO_3 [11, 12]. So far, various researchers have been investigating transition metal ions as dopants to study the structural, electrical and band edge properties of WO_3, including Mo [13], Co [14], Ni [15], Fe [16]. Cu [17, 18] Mn, [19] and Cd [20]. Moreover, various studies have been conducted co-doping transition metal ions tomodify

optoelectricalproperties of WO_3nanoparticles. For instant, S Mohammadi *et al* investigated the effects of pure, Zn, Cu, co-doping Zn and Cu in WO_3nanoparticles prepared by using both precipitation and co-precipitation methods for the application of photocatalytic and antibacterial activity. They found that the co-doping WO_3 nanoparticles have higher photocatalytic degradation of gentamicin than other sample [21]. Albalshi *et al* investigated the electrochemical properties of Ti and Zn co-doped WO_3 thin films synthesized by the sol-gel method [22]. Furthermore, compared to a single doped WO_3 thin film, co-doped film has improved electrochemical and electrochromic properties as well as higher electrochemical stability [22]. N Boonprakob *et al* investigated photocatalytic for removal of hexavalent chromium using Ag and Cu co-doped WO_3 nanoparticles synthesized by using a simple co-precipitation approach [23]. This co-doping effect has higher photocatalytic reduction under visible light irradiation than un-doped [23].

To synthesize WO_3 nanostructures, researchers have used different synthesis methods, for example sol-gel [24], microwave irradiation [25], co-precipitation [26], spray pyrolysis [27], and hydrothermal [28]. Among them, the co-precipitation method is the simplest, cost-effective, the highest purity, and has good uniformity. To our knowledge, no studies have examined pure WO_3, 5% Ni:WO_3 and (2%Ni+5%Cu):WO_3, (3%Ni+5%Cu):WO_3, and 5% (Cu:Ni) co-doped WO_3 nanoparticles by using environmental friendly co-precipitation method. The objective of this work is to give an insight on how the mono doped and co-doped can affect the structure, electrical and optical properties of WO_3 nanoparticles. The obtained results are suggested that the prepared materials are good candidates for solar cell applications.

2. Experimental procedure

2.1. Synthesis of pure, mono and Co- doped (Cu,Ni) WO_3 nanoparticles (NPs)

Pure WO_3, 5%Ni:WO_3 (mono) and (2% Cu+5%Cu):WO_3, (3% Cu+5%Ni):$WO_3$and 5%(Cu:Ni) co-doped WO_3 nanoparticle were synthesized by simple chemical co-precipitation method. The precursors used in the synthesis were sodium tungstates dehydrate, copper (ii) nitrate trihydrate, and nickel nitrate hexahdrate as starting materials., while aqueous HCl used to adjust the pH of the solution and NaCl as capping agent. In a typical synthesis appropriate amount of sodium tungstate dihydrate was dissolved in 100 ml of distilled water. In a closed-necked flask, the solution was vigorously stirred for 30 min with a magnetic stirrer. After 30 min appropriate amount of NaCl was added to the solution then stirred until a homogeneous solution was formed. Then 37% aqueous HCl solution was also added to the above solution drop wise under constant stirring until the pH was attained to 1 and then the solution continues stirred and heated for one hrs at 100 °C. Afterwards, the solution aged for 24 h and then centrifuged to the obtained precipitates. The obtained precipitates were washed several times with distilled water and ethanol to remove excess sodium and chlorine ions then dried in an electric oven at 100 °C overnight. Finally, the obtained powder was calcined at 500 °C for 3 h in order to obtain WO_3 nanoparticles. The 5% Ni:WO_3 and (2% Cu+5%Cu):WO_3, (3% Cu+5%Ni):$WO_3$and 5%(Cu:Ni) co-doped WO_3 nanoparticles have synthesized by chemical co- precipitation method with different weight percentage of 2%, 3%, and 5% for Cu and fixed amount 5% for Ni using the same procedure explained above. The all the obtained samples were used for different characterization.

2.2. Characterization techniques

The phase purity and structure of the pure, mono and co-doped WO_3 nanoparticles were analyzed by XRD-7000 x-ray difractometer maxima with Cu Kα radiation ($\lambda = 0.15406$ nm). The presence of different functional groups in the sample was confirmed by FTIR spectrophotometer (PerkinElmer, Model: Spectrum Two). SEM and UV–Vis Spectroscopy (Model: UV-3600 Plus) were used to characterize the morphological information and optical properties of the samples. Room temperature photoluminescence (PL) spectra were performed by a Fluoromax-4 Spectrofluorometer in the excitation wavelength of 350 nm using a 40 W Xenon arc lamp. The current-voltage characteristics of the junctions were measured using a Keithley source meter unit (model: 2400) in the dark at room temperature.

3. Results and discussion

3.1. XRD analysis

The prepared samples were analyzed by x-ray diffraction using the CuKα wavelength of 0.15406 nm. Figure 1(a) shows the XRD of pure WO_3, 5% Ni:WO_3(2% Cu+5%Cu):WO_3, (3% Cu+5%Ni):WO_3 and 5%(Cu:Ni) co-doped WO_3 nanoparticles. The XRD result confirmed that the prepared samples had an orthorhombic crystal structure of with space group P and lattice parameter a = 7.3840 Å, b =7.5120 Å, and c =3.8460 Å and $\alpha = \beta = \gamma = 90$ °C. The result is in a good agreement with the standard JCPDS card No. 020-1324. The incidence of sharp and number of diffraction peaks revealed the polycrystalline nature of the prepared

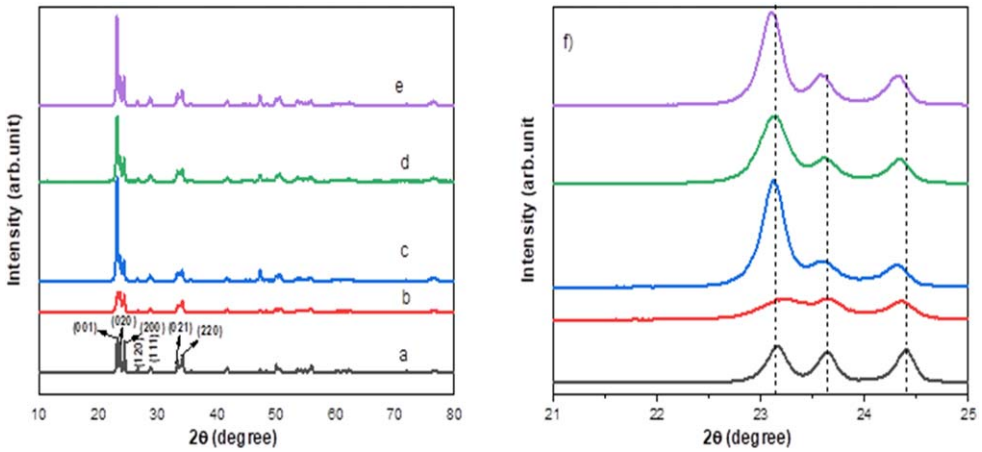

Figure 1. XRD pattern for (a) pure WO_3, (b) 5%Ni:WO_3, (c) (2% Cu+5%Cu):WO_3, (d) (3% Cu+5%Ni):WO_3, (e) 5%(Cu:Ni) co-doped WO_3 nanoparticles. (f) Change in (001), (020) and (200) peaks positions with dopant concentrations.

nanomaterials. No impurity peaks of Ni and Cu were observed from the XRD diffraction pattern which implies a successfully incorporations of Ni^{2+} and Cu^{2+} ions into the WO_3 lattice. As demonstrated in figure 1 the intensity of co–doped (Ni:Cu) WO_3 nanoparticles increased in the plane (001) when compared to 5% Ni:WO_3 and pure WO_3 nanoparticles. This is due to the fact that (Ni:Cu) co-doping improves the development rate of WO_3 nanoparticles and gives them a higher degree of crystallinity than 5% Ni:WO_3 and pure WO_3, resulting in sharper diffraction peaks in XRD. The intensity of 5% Ni doped WO_3 nanoparticles is lower than that of pure WO_3 nanoparticles. As result clearly indicate that the successful incorporation of 5% Ni has the WO_3 matrix.

The crystallite sizes for the prepared NPs were analyzed from the three most prominent diffraction peaks of (001), (020) and (200) planes using the Debye Scherer relation shown in equation (1).

$$D = \frac{K\lambda}{\beta COS\theta} \tag{1}$$

Where, D is average crystallite size obtained from the three dominant peak, K is constant for the shape factor nearly equal to 0.9, λ is the wavelength of x-ray used (CuKα, 0.15406 nm), β is the full width at half maximum and θ is the angel of diffraction of three do peak.

The average crystallite size was calculated by using the (001), (020) and (200) peaks of WO_3 to be 46 nm; 25 nm for 5% Ni:WO_3 furthermore, the crystalline size, it was decreased from 35 nm to 40 nm for various concentration of Cu at 2 wt.%,3 wt.%, 5 wt.% and fixed in Ni of 5 wt.% doped WO_3 respectively. It is indicated that Cu^{2+} and Ni^{2+} ions substituted in the W^{6+} ions lattice site of orthorhombic structure and then the crystallite size was reduced by dopant concentration [29]. The expanded version of XRD (figure 1(f)) clearly shows the slight peak position shifts of (001), (020), (200) planes to the lower diffraction angles when compared to the pure WO_3 NPs. This peak shift to the lower angle for doped NPs indicates that the lattice parameters are slightly varied than the pure WO_3 and a successful substitution Ni^{2+} and Cu^{2+} ions onto the host lattice [30]. This can be associated to the smaller ionic radii difference between the host W (0.62 Å) and dopant 0.60 Å for Ni and 0.73 Å for Cu ions [31, 32].

As shown in table 1, the unit cell volume of WO_3 NPs co-doped with fixed nickel and varying copper amounts decreased with dopant concentration implies that substitution of Cu and Ni ions in the lattice site, as similar phenomena have been reported [33]. It is also observed that the value of the dislocation density of undoped WO_3 NPs has the lowest value as compared to the doped sample, shown in table 1. This indicates that Cu^{2+} and Ni^{2+} co-doping deteriorate the WO_3 crystal structure. Table 1 also reveals that the micro-strain and crystallite size have a strong relationship. The differing ionic radius of W^{6+}, Cu^{2+}, and Ni^{2+} ions, which enhance the micro-strain during the substitution of W ions by both Cu and Ni ions, could explain these changes in micro-strain with crystal size. As a result, dopant concentrations diminish the development rate and crystallinity of WO_3 NPs, and crystal size increases produce a decrease in the strain [34, 35].

The from the XRD peaks the lattice parameters for the orthorhombic crystal structure was calculated by using equation (2):

$$\frac{1}{d^2} = \frac{h^2}{a^2} + \frac{k^2}{b^2} + \frac{l^2}{c^2} \tag{2}$$

Where d is the interplanar spacing; a, b, c are the lattice parameters and h, k, l are the Miller indices. The dislocation density (δ) is the length of dislocation lines per unit volume of the crystal. The defect in the crystal

Table 1. XRD parameters of the prepared nanoparticles with fixed Ni and different Cu concentrations.

Concentrations	Crystallite size (nm)	Dislocation density ($\times 10^{-3}$) lines/m^2	Strain ($\times 10^{-3}$) lines^{-2} m^{-4}	Lattice parameters (Å)			Volume of unit cell
				a	b	c	v = a*b*c(Å)^3
Pure WO_3	46	0.4726	4.6025	7.3053	7.5375	3.8452	211.73
5% Ni:WO_3	25	1.60	16.6950	7.3108	7.5789	3.8371	212.61
2%Cu+5%Ni:WO_3	37	0.7305	6.3924	7.3134	7.5231	3.8375	211.13
3%Cu+5%Ni:WO_3	35	0.8163	6.5447	7.3030	7.5168	3.8366	210.61
5%(Cu:Ni):WO_3	40	0.625	5.2226	7.3076	7.5323	3.8408	211.41
JCPDS (020-1324).			7.3840	7.5120	3.8460	213.33	

structure of WO_3 nanoparticles is measured by the dislocation, and the presence of this strongly influences the properties of the sample. The dislocation density can also be calculated from the equation (3):

$$\delta = \frac{1}{D^2} \tag{3}$$

Where δ is dislocation density and D is the average crystallite size of the sample.

The micro-strian (ε) can be calculated by the following equation [36].

$$\text{Micro-strain } (\varepsilon) = \frac{\beta}{4 \tan \theta} \tag{4}$$

3.1.1. UV–visible diffusion reflectance.

The UV–vis spectroscopy measurements were taken to assess the influence of 5% Ni:WO_3, 2% Cu +5% Ni :WO_3, 3% Cu + 5% Ni :WO_3 and 5% (Cu :Ni) co-doped on WO_3 NPs. Figures 2(a)–(f) shows the reflectance spectra and optical band gap of all WO_3 samples. Figure 2(f) shows all WO_3 samples have minimum reflectance in the UV region. In the entire sample in the visible region, the reflectance increases, but all the co-doped sample has higher reflectance than the 5% Ni:WO_3 and pure WO_3 nanoparticles. The optical band gap energy of WO_3 nanoparticles were analyzed by using Kubelka–Munk function relation equation (5) [26, 37].

$$F(R) = \frac{(1 - R)^2}{2R} \tag{5}$$

Where F(R) is known as kubelka–munk function and R is the reflection of the materials. The indirect band gap energy of the sample can be found by plotting $(F(R)h\upsilon)^{1/2}$versus energy ($h\upsilon$) as shown in the figures 2(a)–(e). The figures 2(a)–(e) indicates that pureWO_3 nanoparticles has the optical band gap of about 2.80 eV which is decreased to 2.63 eV for 5% Ni: WO_3, 2.75 eV for (2% Cu + 5% Ni):WO_3, 2.77 eV for (3% Cu + 5% Ni):WO_3 and 2.73 eV for 5% (Cu: Ni) co-doped WO_3 nanoparticles. The crystal size and dopant content increases the optical band gap energy decrease. Therefore, the reduction in the optical band gap energy of WO_3 is due to the induced defect energy levels near to the conduction and valence band by Cu and Ni ions substitutions in lattice site of orthorhombic structure. However, the electrical transition from the filled valence band to the bottom of the conduction band occurs due to a higher number of defects [38]. This implies that as (Ni,Cu) is co-doped into the WO_3 lattice, defect states are formed, causing the band gap to narrow [39]. The band gap narrow due to there is more light absorption in the visible area, and which can improve the performance of optoelectronic devices.

3.1.2. Photoluminescence (PL) studies

Figure 3 shows the room-temperature PL emission spectra of the prepared samples at an excitation wavelength of 350 nm. The emission spectra of pure WO_3, 5% Ni, WO_3, (2% Cu+5% Ni): WO_3, (3% Cu+5% Ni): WO_3 and 5% (Cu: Ni) co-doped WO_3 nanoparticles are all in the visible region.

The greater emission spectrum in the (Ni,Cu) co-dopant has a higher percentage of surface oxygen vacancy. The emission spectra of pure WO_3, 5%Ni:WO_3,(2% Cu+5%Ni):WO_3,(3% Cu+5% Ni):WO_3 and 5%(Cu:Ni) co-doped WO_3 nanoparticles were exhibited strong emission peaks centered at 431 nm related to violet emission, 440 nm and 445 nm related to blue emission, 494 nm, 500 nm related to blue -green emission, 512, 518, 523, 525, 532, 535, 536, and 547 nm related to green emission, 610 nm related to orange emission and 621, 662 nm and 672 nm related to red emission. These different emission peaks may be due to an electron transition in WO_3's band gap mediated by the defect energy level generated from oxygen vacancies and tungsten

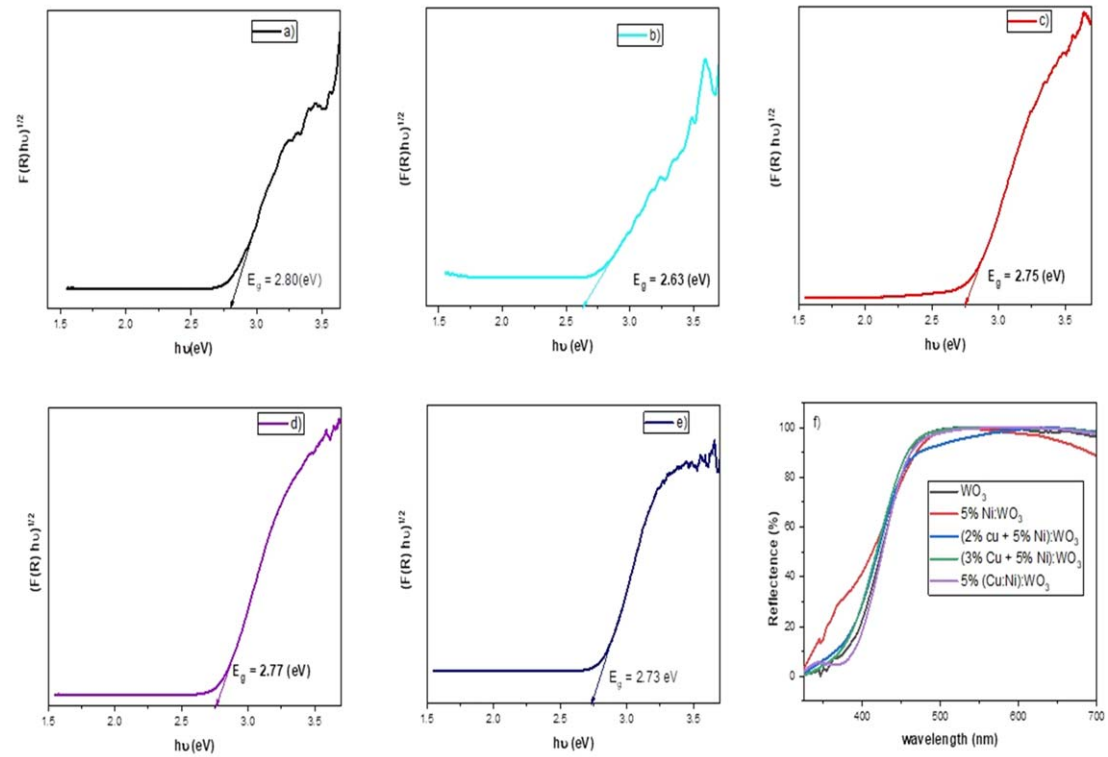

Figure 2. The optical band gap of (a) pure WO_3, (b) 5% Ni:WO_3, (C) (2% Cu+5% Ni):WO_3, (d) (3% Cu+5% Ni):WO_3 (e) 5% (Cu:Ni) co-doped WO_3 nanoparticles. (f) UV–Vis Diffuse reflectance spectra of all sample.

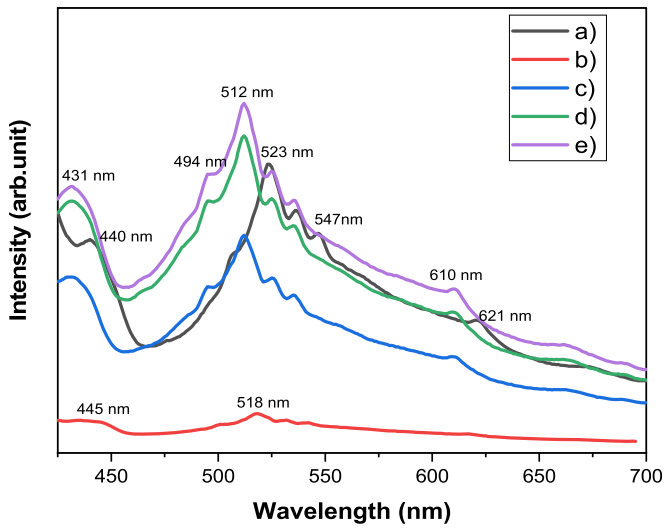

Figure 3. Photoluminescence spectra of (a) pure WO_3, (b) 5% Ni:WO_3, (c) (2%Cu+5% Ni):WO_3, (d) (3% Cu+5% Ni):$WO_3$and (e) 5% (Cu:Ni) :WO_3 nanoparticles.

interstitials [40]. The broad and high intensity peaks observed at 431 nm, can be assigned to recombination free excitons, which are referred to as near band edge emission (NBE) [41]. This originated from the band-to-band transition and corresponds band gap energies of 2.87 eV, respectively, which are consistent with band gap energies derived from UV reflectance spectra. The blue emission peaks at 440 nm and 445 nm are attributed to singly ionized tungsten vacancies [42]. The blue-green emission peaks at 494 and 500 nm due to a surface defects in the WO_3 NPs corresponding to the transition between oxygen vacancy and oxygen interstitial defect or lattice defects related to oxygen and tungsten vacancies [43]. The green emission peaks observed at 2.42 eV, 2.39 eV, 2.37 eV, 2.36 eV, 2.33 eV, 2.31 eV, 2. 26 eV energy bands probably due to defect energy levels which are responsible for oxygen interstitial and vacancies, tungsten interstitial and vacancies, Cu^{2+} and Ni^{2+} ions

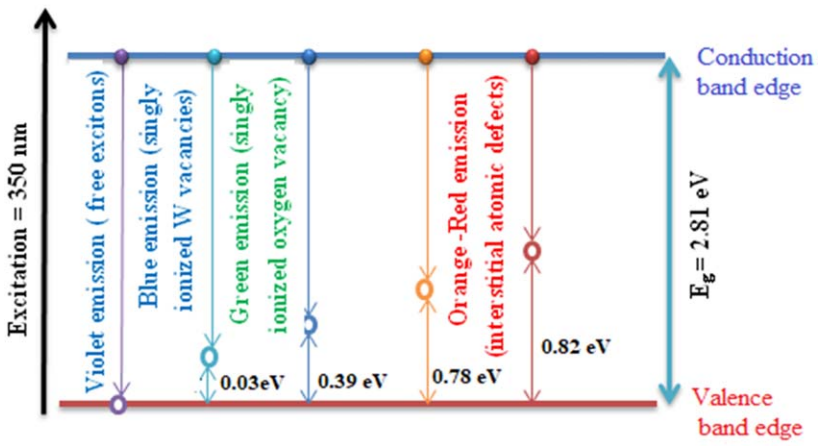

Figure 4. The band gap structure, defect energy levels and different specific emission lines of undoped, mono and Co- doped WO_3 nanoparticles.

impurity and, oxygen antisites [44–48]. The orange-red emission originated from by transitions associated with interstitial atomic defects such as oxygen vacancy and tungsten interstitial [42]. These findings are similar works reported in the literatures [49]. Pure WO_3 and 5% Ni:WO_3 nanoparticles exhibit lower intensity than (Ni: Cu) co-doped WO_3 samples due to a lack of crystallinity [50]. The lower the PL intensity; the lower the recombination rate of photo-induced electron-hole pairs [51]. The increased PL emission intensity was attributed to electron-hole recombination caused by surface imperfections or oxygen vacancies [52]. As a result of the higher growth and more intense PL emission peak observed in the Cu and Ni co-doped WO_3 samples. The PL emission peak of co-doped WO_3 samples shifts to the lower wavelength side and has a distinct intensity because of the substitution of W^{+6} by Ni^{2+} and Cu^{2+} ions into the host WO_3 unit cell lattice site. As the WO_3 nanoparticles were synthesized in an aqueous solution a high density of oxygen vacancies might be expected. The oxygen vacancy itself may be neutral, singly ionized or doubly ionized [49, 53]. These oxygen vacancies and interstitial atomic defects form a number of trap states which are responsible for the various PL emissions in the visible region. similarly, as shown in figure 3, the incorporations of Ni^{2+} and Cu^{2+} ions into the WO_3 matrix resulted as a development of more new trapping centers. Based on the above discussions the proposed emission mechanisms of the generalized band gap structure and specific defect levels emissions of the prepared samples are illustrated in figure 4.

3.1.3. Fourier transforms infra-red (FTIR) analysis

The FTIR spectroscopy was studied to the information about the surface chemistry and chemical quality of WO_3 nanoparticles. Figure 5 shows the FTIR analysis of pure WO_3, 5% Ni:WO_3, (2%Cu+5% Ni):WO_3, (3% Cu+5% Ni):WO_3 and 5% (Cu:Ni):WO_3NPs. The observed band located at 1409 cm^{-1} represented to bending modes of O–H groups and the band located at 2955 to 3683 cm^{-1} maybe represented to the stretching modes of O–H group in water or hydroxyls [32, 54]. Furthermore, the broad band observed at 550 to 1050 cm^{-1} is linked with the O–W–W stretching mode [32, 54]. The presence of WO_3 stretching mode and absence of Ni and Cu oxide related mode further support that Ni^{2+} and Cu^{2+} ions are successfully doped WO_3 crystal structure. The orthorhombic crystal WO_3 nanoparticle had no impurities detected in the FTIR investigation, which was verified by the XRD data.

3.1.4. Surface morphology analysis

The morphology and histogram results of pure WO_3, 5% Ni:WO_3, and 5% (Ni: Cu) co-doped WO_3 nanoparticles are shown in figures 6(a)–(f). As demonstrated in figures 6(a)–(c), the morphology of all samples is uniform and densely packed. The particles were clearly agglomerated in the SEM images. From the SEM images it is easily observed that doping with Ni and Cu plays a significant role on the morphological nature of the nanocrystalline of the prepared samples. The surface morphology is also impacted by the dopant element, indicating that W^{6+} has been replaced in the WO_3 lattice by transition metal ions, as shown by SEM micrographs. The average particle size distribution of WO_3, 5% Ni, and 5% (Ni: Cu) co-doped WO_3 was obtained by analyzing the SEM image using the software ImageJ as shown in figures 6(d)–(f). The histograms represent WO_3 nanoparticles with an average diameter of about 225 nm. However, the addition of Ni^{2+} influence the size morphology in which of average particles size distribution of the nanoplates is decreased from 225 nm to 138 nm due to divalent nickel ions restrict the growth of WO_3 and lead to growing in the nanoplate

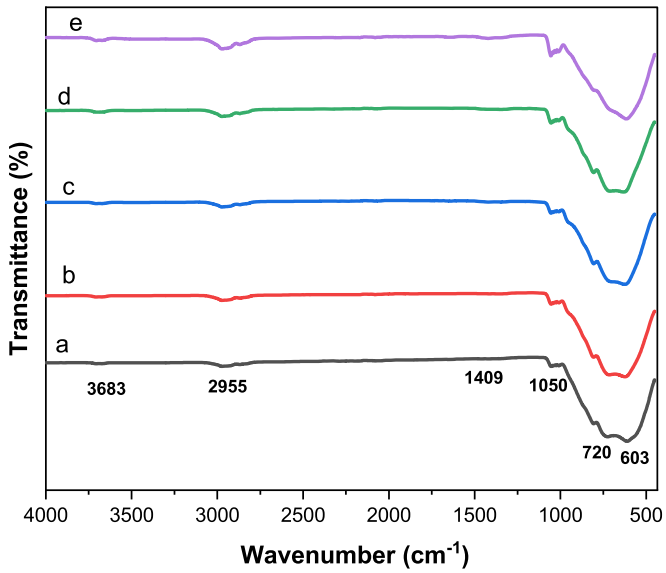

Figure 5. FTIR analysis of (a) pure WO_3, (b) 5% Ni:WO_3, (c) (2% Cu+5%Ni):WO_3, (d) (3% Cu+5% Ni):WO_3 and (e) 5% (Cu:Ni) co-doped WO_3 nanoparticles.

direction shown in figure 6(b) [55]. This decreased the average diameter which is a good agreement with average crystalline size calculated from the XRD. When both Ni^{2+} and $Cu^{2+}$the dopant precursor concentration the morphology may be attributed to resulting in the change of surface feature from nanoplates shape to both nanorods and nanoplates shows in figure 6(c). The Ni and Cu co-doped WO_3 nanoparticles increase the diameter from 225 to 252 nm shown in figure 6(f). These co-doping change both the shape and size of the WO_3 nanoparticles.

3.1.5. I–V characteristic studies

The electrical properties were carried outunder dark condition at room temperatureof pure WO_3, 5% Ni:WO_3 and (2% Cu+5% Ni):WO_3,(3% Cu+5% Ni):WO_3 and 5% (Cu/Ni) co-doped WO_3 thin film. The prepared samples were used to deposit on glass substrate by simple spin coating method after dissolving in DFM. Then the spin coated film was dried at 100 °C for 2 h in an oven, and the metal contact was made over the prepared film using sliver past. The result of the I-V characteristics measured for the sample exhibits a good ohmic behavior as shown in figure 7. The resistivity of the sample was calculated by using equation (5) and as shown table 2.

$$\rho = \frac{R \times A}{L} \tag{6}$$

Where, ρ is the resistivity of the film (Ω. cm), R is the resistance (Ω), A is the area of active layer (cm^{-2}) and L is the length in (cm).

The resistivity of calculated value found to decrease from 6.3×10^{-3} Ω.cm for WO_3 film to 2.9×10^{-3} Ω.cm for 5% (Cu:Ni):WO_3 and 0.63×10^{-3} Ω.cm for 5% Ni: WO_3 thin film. This demonstrates that altering the dopant concentration in the lattice increases the electrical conductivity of WO_3 thin films by increasing carrier charge mobility. The amount of dopant in the WO_3 unit cell lattice can generate crystallographic defects, alter the electronic structure, and reduce the electrical characteristics of the (2% Cu + 5% Ni):WO_3 and (3% Cu + 5% Ni):WO_3 thin films related to pure WO_3.

These findings of similar work with previous literature results were obtained by [56–58]. As a result, the electrical properties of 5% Ni:WO_3 NPs were found to better performance than Ni and Cu co-doped WO_3 and undoped samples. It is also observed that the resistance of the synthesized thin films decreases as the dopant concentration increases. The prepared samples show good ohmic properties and are good candidates for solar cell window applications.

4. Conclusions

Pure WO_3, 5%Cu:WO_3, (2% Cu + 5% Ni): WO_3, (3% Cu + 5% Ni): WO_3, and 5% (Ni:Cu):WO_3 nanoparticles were successfully synthesized by co-precipitation methods. The structural, optical, and electrical properties of the prepared nanomaterials were investigated. The formation of the nanocrystalline orthorhombic structure of WO_3 was confirmed by XRD. Moreover, average crystalline size, microstrain, unit cell volume and

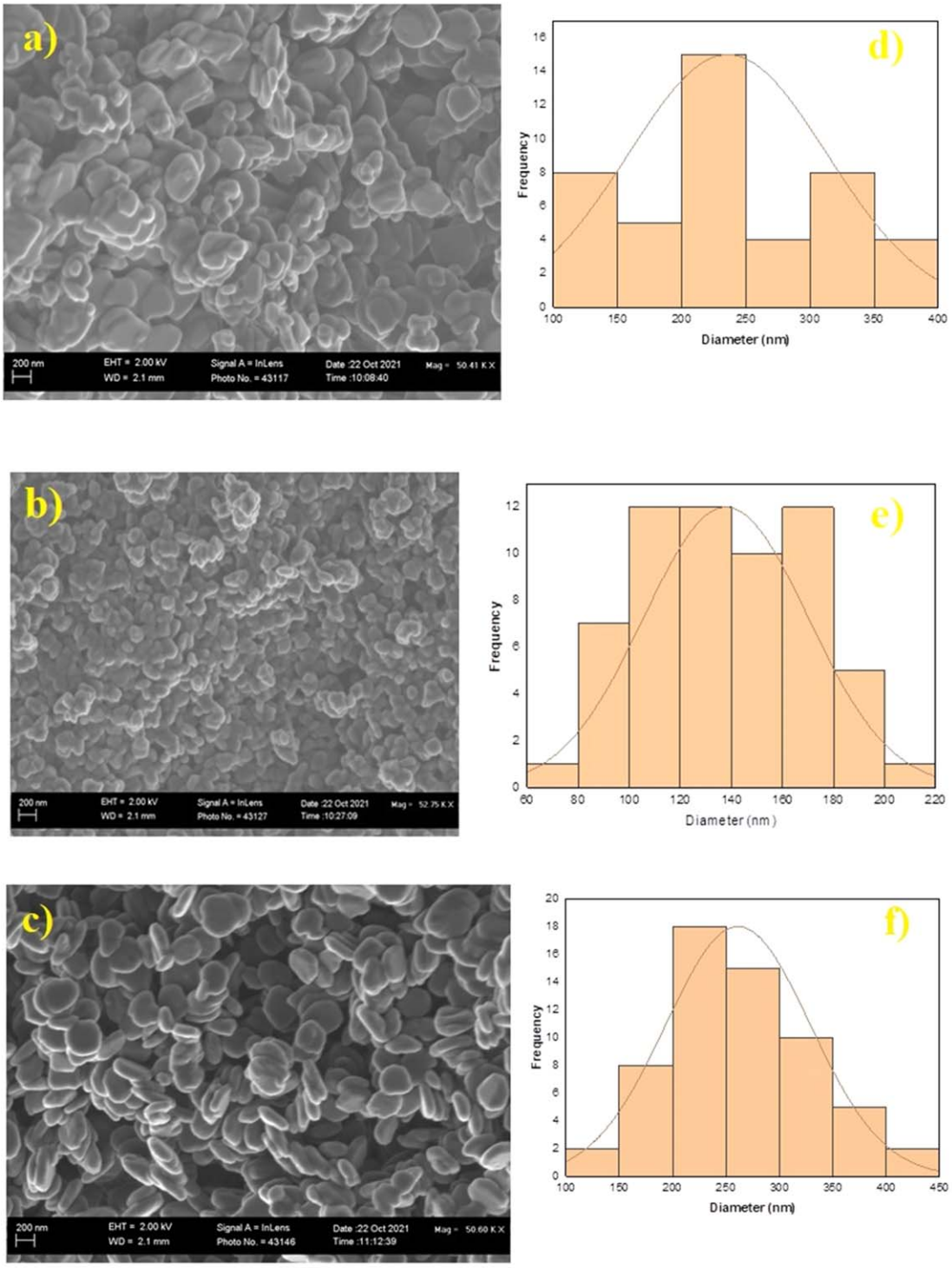

Figure 6. SEM images of (a) pure WO_3 (b) 5% Ni: $WO_3$and (C) 5% (Cu:Ni):WO_3 NPs and the average grain size of (d) pure WO_3, (e) 5% Ni:WO_3, (f) 5% (Cu:Ni):WO_3 NPs.

lattice parameters were significantly influenced by the dopant concentrations. The UV-Vis analyses revealed that the band gaps of the prepared samples decreased as the dopant concentrations increased. Various PL emissions in visible region were observed due to defects from a number of trap states. The increased intensity of the PL emission peak at 431 nm, 440 nm, 512 nm, and 523 nm of pure WO_3 and (Ni: Cu) co-doped WO_3 samples was attributed to the high electron–hole recombination caused by nanoplates with little rod morphology. The SEM micrographs confirmed that the prepared samples have both nanoplate and nanorod shapes and are agglomerated irrespective of the dopants. The result of the I-V characteristics measured for the sample exhibits a good ohmic behavior and the resistivity decreased with dopant concentration. The obtained results revealed that the prepared materials are suitable for solar cell devices as the window layer.

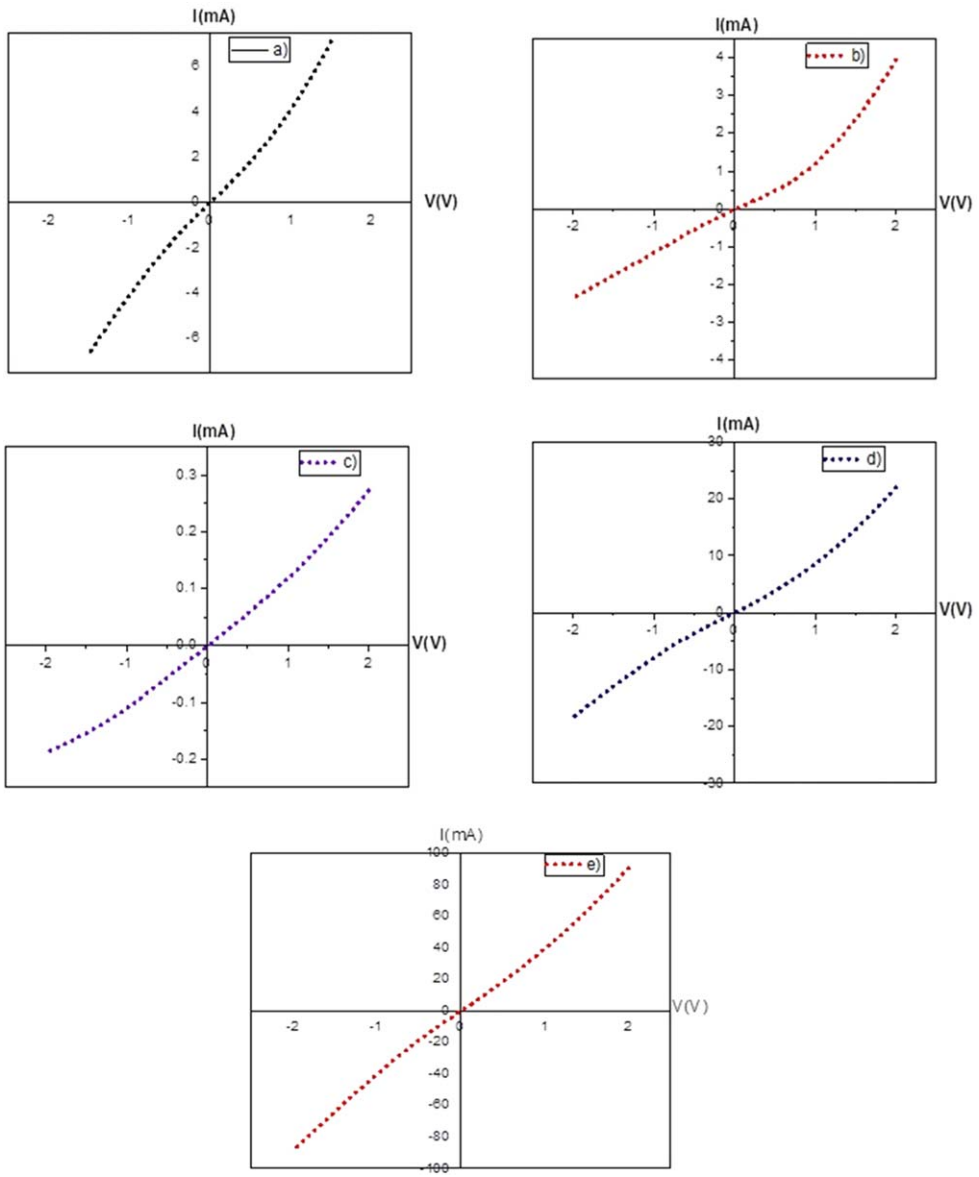

Figure 7. I-V curves of (a) pure WO_3, (b) (2% Cu + 5% Ni): WO_3, (c) (3% Cu + 5% Ni): WO_3, (d) 5% (Ni:Cu): $WO_3$and (e) 5% Ni: WO_3 NPs.

Table 2. Resistivity of the prepared thin films with fixed Ni and different Cu concentrations.

Samples	WO_3	(2% Cu+5% Ni):WO_3	(3% Cu+5% Ni):WO_3	5% Ni:WO_3	5% (Cu:Ni): WO_3
Resistivity (Ω.cm)	6.3×10^{-3}	19.3×10^{-3}	232.5×10^{-3}	0.63×10^{-3}	2.9×10^{-3}

Data availability statement

The data that support the findings of this study are available upon reasonable request from the authors.

ORCID iDs

Fekadu Gashaw Hone https://orcid.org/0000-0002-2332-1750
Dinsefa Mensur Andoshe https://orcid.org/0000-0001-9664-1344
Mulualem Abebe Mekonnen https://orcid.org/0000-0001-9496-5185

References

[1] Fernández-Domene R M, Sánchez-Tovar R, Lucas-Granados B, Roselló-Márquez G and Garcia-Anton J 2017 A simple method to fabricate high-performance nanostructured WO_3 photocatalysts with adjusted morphology in the presence of complexing agents *Mater. Des.* **116** 160–70

[2] Durrani S M A, Khawaja E E, Salim M A, Al-Kuhaili M F and Al-Shukri A M 2002 Effect of preparation conditions on the optical and thermochromic properties of thin films of tungsten oxide *Sol. Energy Mater. Sol. Cells* **71** 313–25

[3] Feng M, Pan A L, Zhang H R, Li Z A, Liu F, Liu H W and Gao H J 2005 Strong photoluminescence of nanostructured crystalline tungsten oxide thin films *Appl. Phys. Lett.* **86** 141901

[4] Granqvist C G 2000 Electrochromic tungsten oxide films: review of progress 1993–1998 *Sol. Energy Mater. Sol. Cells* **60** 201–62

[5] György E, Socol G, Mihailescu I N, Ducu C and Ciuca S 2005 Structural and optical characterization of WO_3 thin films for gas sensor applications *J. Appl. Phys.* **97** 093527

[6] Kim K, Seo C, Cheong H and Lee S H 2006 Photochromic mechanism in a-WO_3 thin films based on Raman spectroscopic studies *J. Korean Phys. Soc.* **48** 1657–60

[7] Avellaneda C O and Bulhões L O 2003 Intercalation in WO_3 and WO_3: Li films *Solid State Ionics* **165** 59–64

[8] Granqvist C G (ed) 1995 *Handbook of Inorganic Electrochromic Materials* (Amsterdam: Elsevier)

[9] Kalantar-Zadeh K, Vijayaraghavan A, Ham M H, Zheng H, Breedon M and Strano M S 2010 Synthesis of atomically thin WO_3 sheets from hydrated tungsten trioxide *Chem. Mater.* **22** 5660–6

[10] Su J, Guo L, Bao N and Grimes C A 2011 Nanostructured $WO_3/BiVO_4$heterojunction films for efficient photoelectrochemical water splitting *Nano Lett.* **11** 1928–33

[11] Upadhyay S B, Mishra R K and Sahay P P 2014 Structural and alcohol response characteristics of Sn-doped WO_3nanosheets *Sensors Actuators* B **193** 19–27

[12] Kalanur S S, Yoo I H, Eom K and Seo H 2018 Enhancement of photoelectrochemical water splitting response of WO_3 by means of Bi doping *J. Catal.* **357** 127–37

[13] Pooyodying P, Ok J W, Son Y H and Sung Y M 2021 Electrical and optical properties of electrochromic device with WO_3: Mo film prepared by RF magnetron Co-sputtering *Opt. Mater.* **112** 110766

[14] Mehmood F, Iqbal J, Jan T, Gul A, Mansoor Q and Faryal R 2017 Structural, photoluminescence, electrical, anti-cancer and visible light driven photocatalytic characteristics of Co doped WO_3 nanoplates *Vib. Spectrosc.* **93** 78–89

[15] Dakhel A A and Ashoor H 2019 Synthesis of semiferromagnetic Ni-doped WO_3 nanoparticles by precipitation method: evaluation of effect of treatment in hydrogen gas *Mater. Chem. Phys.* **230** 172–7

[16] Mehmood F, Iqbal J, Jan T and Mansoor Q 2017 Structural, Raman and photoluminescence properties of Fe doped WO_3nanoplates with anti-cancer and visible light driven photocatalytic activities *J. Alloys Compd.* **728** 1329–37

[17] Mehmood F, Iqbal J, Gul A, Ahmed W and Ismail M 2017 Facile synthesis of 2D Cu doped WO_3nanoplates with structural, optical and differential anti-cancer characteristics *Physica* E **88** 188–93

[18] Tudorache F 2018 Investigations on microstructure, electrical and magnetic properties of copper spinel ferrite with WO_3 addition for applications in the humidity sensors *Superlattices Microstruct.* **116** 131–40

[19] Mohan L, Avani A V, Kathirvel P, Marnadu R, Packiaraj R, Joshua J R and Saravanakumar S 2021 Investigation on structural, morphological and electrochemical properties of co-precipitation synthesis of Mn doped WO_3 nanoparticles for supercapacitor applications *J. Alloys Compd.* **882** 160670

[20] Kalaiarasi S, Christy H K S and Muthuchudarkodi R R 2020 Optical, structural and morphological characterization of cadmium ion doped WO_3 nanoparticles *Journal of Advanced Scientific Research* **11** 155–60

[21] Mohammadi S, Sohrabi M, Golikand A N and Fakhri A 2016 Preparation and characterization of zinc and copper co-doped WO_3 nanoparticles: application in photocatalysis and photobiology *J. Photochem. Photobiol.*, B **161** 217–21

[22] Albalshi M A M 2016 Electrochemical properties of Sol-gel WO_3 films Co-doped with Ti and Zn *Doctoral dissertation* An-Najah National University

[23] Boonprakob N, Channei D and Zhao C 2021 Heterogeneous photocatalytic reduction of hexavalent chromium by modified Ag, Cu co-doped tungsten oxide nanoparticles *J. Aust. Ceram. Soc.* **57** 743–54

[24] Saasa V, Malwela T, Lemmer Y, Beukes M and Mwakikunga B 2020 The hierarchical nanostructured Co-doped WO_3/carbon and their improved acetone sensing perfomance *Mater. Sci. Semicond. Process.* **117** 105157

[25] Hariharan V, Aroulmoji V, Prabakaran K, Gnanavel B, Parthibavarman M, Sathyapriya R and Kanagaraj M 2016 Magnetic and electrochemical behaviour of cobalt doped tungsten oxide (WO_3) nanomaterials by microwave irradiation method *J. Alloys Compd.* **689** 41–7

[26] Mehmood F, Iqbal J, Jan T, Gul A, Mansoor Q and Faryal R 2017 Structural, photoluminescence, electrical, anti-cancer and visible light driven photocatalytic characteristics of Co doped WO_3 nanoplates *Vib. Spectrosc.* **93** 78–89

[27] Bertus L M, Faure C, Danine A, Labrugère C, Campet G, Rougier A and Duta A 2013 Synthesis and characterization of WO_3 thin films by surfactant assisted spray pyrolysis for electrochromic applications *Mater. Chem. Phys.* **140** 49–59

[28] Tehrani F S, Ahmadian H and Aliannezhadi M 2020 Hydrothermal synthesis and characterization of WO_3 nanostructures: effect of reaction time *Mater. Res. Express* **7** 015911

[29] Sivakarthik P, Thangaraj V and Parthibavarman M 2017 A facile and one-pot synthesis of pure and transition metals (M = Co & Ni) doped WO_3 nanoparticles for enhanced photocatalytic performance *J. Mater. Sci., Mater. Electron.* **28** 5990–6

[30] Wu X, Wei Z, Zhang L, Zhang C, Yang H and Jiang J 2014 Synthesis and characterization of Fe and Ni co-doped ZnO nanorods synthesized by a hydrothermal method *Ceram. Int.* **40** 14635–40

[31] Mehmood F, Iqbal J, Ismail M and Mehmood A 2018 Ni doped WO_3 nanoplates: an excellent photocatalyst and novel nanomaterial for enhanced anticancer activities *J. Alloys Compd.* **746** 729–38

[32] Deepa B and Rajendran V 2018 Pure and Cu metal doped WO_3 prepared via co-precipitation method and studies on their structural, morphological, electrochemical and optical properties *Nano-structures & Nano-objects* **16** 185–92

[33] Phaomei G, Rameshwor Singh W and Ningthoujam R S 2011 Solvent effect in monoclinic to hexagonal phase transformation in LaPO4:RE (RE = Dy3+, Sm3+) nanoparticles: photoluminescence study *J. Lumin.* **131** 1164–72

[34] Mishra R K, Kushwaha A and Sahay P P 2014 Influence of Cu doping on the structural, photoluminescence and formaldehyde sensing properties of SnO_2 nanoparticles *RSC Adv.* **4** 3904–12

[35] Mrabet C, Boukhachem A, Amlouk M and Manoubi T 2016 Improvement of the optoelectronic properties of tin oxide transparent conductive thin films through lanthanum doping *J. Alloys Compd.* **666** 392–405

[36] Rajesh Kumar B and Hymavathi B 2017 X-ray peak profile analysis of solid-state sintered alumina doped zinc oxide ceramics by Williamson–Hall and size-strain plot methods *Journal of Asian Ceramic Societies* **5** 94–103
[37] Li X, Mu W, Xie X, Liu B, Tang H, Zhou G and Luo S 2014 Strontium adsorption on tantalum-doped hexagonal tungsten oxide *J. Hazard. Mater.* **264** 386–94
[38] Baraneedharan P, Hussain S I, Dinesh V P, Siva C, Biji P and Sivakumar M 2015 Lattice doped Zn–SnO_2 nanospheres: a systematic exploration of dopant ion effects on structural, optical, and enhanced gas sensing properties *Appl. Surf. Sci.* **357** 1511–21
[39] Ahmed A, Ali T, Naseem Siddique M, Ahmad A and Tripathi P 2017 Enhanced room temperature ferromagnetism in Ni doped SnO_2 nanoparticles: a comprehensive study *J. Appl. Phys.* **122** 083906
[40] Pascariu Dorneanu P, Airinei A, Grigoras M, Fifere N, Sacarescu L, Lupu N and Stoleriu L 2016 Structural, optical and magnetic properties of Ni doped SnO_2 nanoparticles *Jour. alloys and Compou* **668** 65–72
[41] Meenakshi M, Gowthami V, Perumal P and Sanjeeviraja C 2014 Effect of RF power on the structuraland optical characterization of (WO3) 0.90 (V2O5) 0.10 thin films *Int. J. ChemTech. Res.* **6** 5412–8
[42] Mishra S K, Srivastava R K, Prakash S G, Yadav R S and Panday A C 2010 Photoluminescence and photoconductive characteristics of hydrothermally synthesized ZnO nanoparticles *Opto-Electron. Rev.* **18** 467–73
[43] Hameed A S H, Karthikeyan C, Ahamed A P, Thajuddin N, Alharbi N S, Alharbi S A and Ravi G 2016 *In vitro* antibacterial activity of ZnO and Nd doped ZnO nanoparticles against ESBL producing *Escherichia coli* and Klebsiella pneumoniae *Sci. Rep.* **6** 1–11
[44] Hu J and Pan B C 2008 Electronic structures of defects in ZnO: hybrid density functional studies *J. Chem. Phys.* **129** 154706
[45] Lee C T 2010 Fabrication methods and luminescent properties of ZnO materials for light-emitting diodes *Materials* **3** 2218–59
[46] Dhanalakshmi J, Iyyapushpam S, Nishanthi S T, Malligavathy M and Padiyan D P 2017 Investigation of oxygen vacancies in Ce coupled TiO_2 nanocomposites by Raman and PL spectra *Adv. Nat. Sci.: Nanosci. Nanotechnol.* **8** 015015
[47] Ding B, Han C, Zheng L, Zhang J, Wang R and Tang Z 2015 Tuning oxygen vacancy photoluminescence in monoclinic Y_2WO_6 by selectively occupying yttrium sites using lanthanum *Sci. Rep.* **5** 1–10
[48] Anbuselvan D and Muthukumaran S 2015 Defect related microstructure, optical and photoluminescence behaviour of Ni, Cu co-doped ZnO nanoparticles by co-precipitation method *Opt. Mater.* **42** 124–31
[49] Mythili N and Arulmozhi K T 2014 Characterization studies on the chemically synthesized α and β phase PbO nanoparticles *Int. J. Sci. Eng. Res.* **5** 412–6
[50] Hirano M and Okamoto T 2018 Synthesis, morphology, and luminescence of $ZnNb_2O_6$ nanocrystals by hydrothermal method *Nano-Structures & Nano-Objects* **13** 139–45
[51] Aamir L 2021 Novel p-type Ag-WO_3 nano-composite for low-cost electronics, photocatalysis, and sensing: synthesis, characterization, and application *J. Alloys Compd.* **864** 158108
[52] Chen D, Shen G, Tang K, Liang Z and Zheng H 2004 AOT-microemulsions-based formation and evolution of $PbWO_4$ crystals *J. Phys. Chem.* B **108** 11280–4
[53] Sahay P P, Mishra R K, Pandey S N, Jha S and Shamsuddin M 2013 Structural, dielectric and photoluminescence properties of co-precipitated Zn-doped SnO_2 nanoparticles *Curr. Appl Phys.* **13** 479–86
[54] Willis H A, Van der Maas J H and Miller R G 1987 *Laboratory methods in vibrational spectroscopy* (New York: Wiley)
[55] Mehmood F, Iqbal J, Jan T and Mansoor Q 2017 Structural, Raman and photoluminescence properties of Fe doped WO_3 nanoplates with anti-cancer and visible light driven photocatalytic activities *J. Alloys Compd.* **728** 1329–37
[56] Serin T, Serin N, Karadeniz S, Sarı H, Tuğluoğlu N and Pakma O 2006 Electrical, structural and optical properties of SnO_2 thin films prepared by spray pyrolysis *J. Non-Cryst. Solids* **352** 209–15
[57] Salah N, Habib S and Azam A 2017 The influence of transition metal doping on the thermoelectric and magnetic properties of microwave synthesized SnO_2 nanoparticles *J. Mater. Sci., Mater. Electron.* **28** 435–45
[58] Soussi L, Garmim T, Karzazi O, Rmili A, El Bachiri A, Louardi A and Erguig H 2020 Effect of (Co, Fe, Ni) doping on structural, optical and electrical properties of sprayed SnO2 thin film *Surfaces and Interfaces* **19** 100467